A local order study of molten $LiNbO_3$ by neutron diffraction

1993 J. Phys.: Condens. Matter 5 4865

(http://iopscience.iop.org/0953-8984/5/28/003)

J. Phys.: Condens. Matter 5 (1993) 4865–4876. Printed in the UK

A local order study of molten $LiNbO_3$ by neutron diffraction

P Andonov†, P Chieux‡ and S Kimura§

† Laboratoire de Magnétisme et Matériaux Magnétiques de Bellevue, 1, place Aristide Briand, 92195 Meudon Cedex, France

‡ Institut Laue–Langevin, 156 X centre de tri, 38042 Grenoble Cedex, France

§ National Institute for Research in Inorganic Materials, I-I Namiki, Tsukuba Ibaraki, 305 Japan

Received 13 July 1992, in final form 11 March 1993

Abstract. The total structure factor $S(Q)$ and the total pair correlation function $G(r)$ of liquid $LiNbO_3$ have been investigated by neutron diffraction. The temperature dependence of the scattered intensity has been measured in the range of momentum transfer 0.3 $Å^{-1} < Q <$ 16.2 $Å^{-1}$ and the range of temperature 1623 K > T > 1490 K including an undercooling domain. A large variation of $S(Q)$ with temperature was never observed. From an analysis of $G(r)$ made with reference to the crystalline $LiNbO_3$ structure, it was possible to confirm a local ordering similar to the crystalline one. The assumption of a change in the Nb coordination in the liquid near solidification is unfounded. The Nb atom remains octahedrally coordinated up to one hundred degrees above the melting point. The values of the first-neighbour distances $r_{1_{Nb-O}}$, $r_{1_{O-O}}$ and $r_{1_{Li-O}}$ and the coordination numbers n_{Li-O} and n_{O-O} can be explained by the presence of NbO_6 octahedra bonded together by Li atoms in the melt.

1. Introduction

Lithium metaniobate $LiNbO_3$ is one of the most interesting materials for optics owing to its electro-optical and non-linear optical properties [1,2]. Single crystals are synthesized from the liquid state by the Czochralski method on an industrial scale. So, in order to seek the best conditions for crystal synthesis, structure sensitive properties such as viscosity, density and surface tension have been measured [3–5]. Near the melting point, anomalous behaviour has been detected, implying that some ordering clusters exist, probably formed by the niobium oxide molecules in the melt. This behaviour might be related to the appearance of subgrain boundaries in the growing crystal [4–6]. The influence of the local order in the melt on the crystallization processes was also studied by high-temperature Raman spectroscopy. Voronko *et al* [7] explain the strong modification of the spectrum by a change of Nb coordination. At high temperature, $\{NbO_4\}$ tetrahedral complexes formed by covalent bonding would be present in the melt and sharing vertices only. A rearrangement of these units would take place in the temperature domain just before solidification to obtain octahedral $\{NbO_6\}$ units as observed in the crystal, which is classified in the family of ilmenite. The ferroelectric phase, belonging to the rhombohedral system with the space group $R3c$, has been resolved by Abrahams *et al* [8] and the thermal expansion of the interatomic bonds was studied by Megaw [9] and compared to those of other niobates belonging to the family of perovskite-related structures. In the paraelectric phase, which appears at the Curie point T_C just a few degrees below the melting point T_m, the space group is changed to $R\bar{3}c$, but the structure was not resolved and T_C not accurately defined since its value is between 1413 K and 1483 K according to different authors [8, 10, 11].

0953-8984/93/284865+12$07.50

Recently a change of the Nb coordination has been ruled out by structural analysis carried out by means of x-ray diffraction [12] which shows a constant Nb coordination at the three studied temperatures: 1548 K, 1573 K and 1598 K. To look again for possible changes in the structure of the melt prior to solidification, we have undertaken an experimental study in which the progressive evolution of the local order is observed *in situ* from 1623 K to 1490 K, using high-temperature neutron diffraction. We report our results, which confirm a local ordering in the melt as in the crystalline state, and no real change of the Nb coordination.

2. Experimental details

The sample was prepared in the NIRIM at Tsukuba. Li_2CO_3 and Nb_2O_5 powders of high purity (99.99%) and natural isotopic abundance were mixed in congruent composition [13], pressed into cylindrical form and calcined at 1000 °C for 5 h. The final rods of sintered $LiNbO_3$ so obtained are identical to those used for the growth of $LiNbO_3$ single crystals by the RF-heated Czochralski method. In view of its high corrosiveness liquid $LiNbO_3$ has to be maintained under an oxidizing air atmosphere in a sealed Pt container. An important density change exists between solid and liquid states ($d_{solid} \simeq 4.63$ g cm^{-3} at 298 K and $d_{liquid} \simeq 3.66$ g cm^{-3} near T_m at 1526 K); so the container dimensions (diameter 12 mm, height 100 mm and wall thickness 0.2 mm) are chosen to accommodate the volume expansion as well as to optimize the neutron diffraction experiment.

These experiments were carried out on the D4B spectrometer at the Institut Laue–Langevin in Grenoble. High temperature was obtained using a cylindrical V heater equipped with radiation shields. Temperature control and monitoring were achieved via two Pt/Pt–Rh thermocouples in contact with the sample base. Crucible and heater were placed in an evacuated bell-jar to minimize air scattering. The wavelength of the monochromatic beam (Cu(200)), zero shift, stability and efficiency of the two ^{3}He multidetectors and instrumental resolution were determined with great accuracy. The angular range of the measurement was maintained within $1.6° \leqslant 2\Theta \leqslant 131.4°$ (2Θ = scattering angle). With a wavelength $\lambda = 0.7064$ Å and $Q = (4\pi \sin\Theta)/\lambda$, the explored Q range extended from 0.27 to 16.26 Å^{-1}. Given the sample scattering power, a complete angular scan of more than 900 points was achieved in about 1 h with a counting accuracy of about 0.2%. Therefore the statistical errors were always small as compared to the effects induced by temperature variation.

The intensities $I_s(2\Theta)$ from the $LiNbO_3$ melt were measured at 16 different temperatures, T decreasing from 1623 K to 1490 K by steps of 20 K at high temperature, then 10 K and finally 3 K near solidification. A large undercooling domain ($\Delta T \simeq 36$ K) was observed, since $T_m = 1526$ K and the onset of crystallization was detected only below 1490 K, where Bragg peaks could be detected. Following the evolution of the first Bragg peak *in situ* during the initial temperature rise (see figure 1), an important decrease of intensity was observed at 1483 K and a sharp outbreak of peak splitting appeared at 1496 K, but we did not investigate the paraelectric phase further. We decided to compare the local order in the liquid to that of the rhombohedral phase which is well documented. For a meaningful comparison of the local interatomic distances between liquid and solid, an estimate of the mean expansion coefficient α_m in the rhombohedral phase is necessary. Assuming isotropic and continuous expansion, α_m is obtained as 3.3×10^{-5} deg^{-1} from the temperature dependence of the first Bragg peak position ($d_{012} = 3.78 \pm 0.02$ Å at 300 K and 3.93 ± 0.02 Å at 1486 K).

The intensities scattered by an empty reference Pt cell of the same dimensions were also measured to study recrystallization effects on warming and then on cooling, at each temperature chosen for the study of the melt.

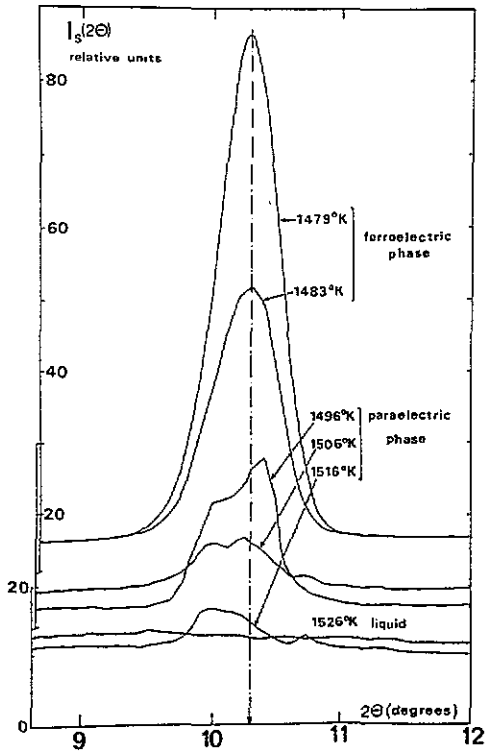

Figure 1. Temperature dependence of the (012) peak in crystalline $LiNbO_3$ near the ferro- to paraelectric *transition.*

The total interference function was obtained using the procedure described elsewhere [14, 15]. The neutron intensities were corrected for background, furnace and container scattering and sample self-absorption using the values of the coherent scattering and absorption cross sections of the three elements as listed in [16] and [17] and reported in table 1. The contribution of multiple scattering ($\sim 15\%$), incoherent and inelastic scattering were subtracted. Then, normalization to the known scattering cross section was achieved in the high-Q domain where the oscillations of the diffracted intensities are small. The steepness of the low-Q data prevents an accurate extrapolation to the thermodynamic limit $S(0)$. A cross check of the data correction and normalization with the value of $S(0)$ obtained from the thermodynamic properties is therefore not possible.

Table 1. Linear total absorption coefficients μ_{total}, coherent scattering length b_{coh} of the various materials, and weights W_{ij}, expressed in % of the partial functions defined in equations (1) and (2).

	$LiNbO_3$ at 1540 K $\Rightarrow$ 0.721_6 cm^{-1}					
	Pt at 1540 K $\Rightarrow$ 1.047_5 cm^{-1}					
μ_{total}	V at 1540 K $\Rightarrow$ 0.518_9 cm^{-1}					
	Li		Nb		O	
b_{coh} (10^{-12} cm)	−1.903		5.805		7.054	
	Li–Li	Nb–Nb	O–O	Li–Nb	Li–O	Nb–O
W_{ij} (%)	0.64	9.82	58.81	−5.03	−12.30	48.05

3. Data processing

The method of analysing the scattering intensity for non-crystalline systems is now well established. Only details relevant to the present work are recalled. Within the formalism of Faber and Ziman [18] generalized to a non-crystalline system with more than two kinds of atom, the total structure factor $S(Q)$ can be related to the partial structure factors and the coherent scattering cross section per atom $d\sigma_{coh}/d\Omega(Q)$ as follows:

$$S(Q) = \left(\frac{d\sigma_{coh}(Q)}{d\Omega} - \langle b^2\rangle - \langle b\rangle^2\right)/\langle b\rangle^2 = \sum_{i=1}^{m}\sum_{j=1}^{m} W_{ij}S_{ij}(Q). \tag{1}$$

In our case $m = 3$ and 1, 2 or 3 are for Li, Nb or O respectively. More explicitly equation (1) can be written as

$$\begin{aligned} S(Q) = {} & (c_1^2b_1^2/\langle b\rangle^2)S_{11}(Q) + (c_2^2b_2^2/\langle b\rangle^2)S_{22}(Q) + (c_3^3b_3^3/\langle b\rangle^2)S_{33}(Q) \\ & + (2c_1c_2b_1b_2/\langle b\rangle^2)S_{12}(Q) + (2c_2c_3b_2b_3/\langle b\rangle^2)S_{23}(Q) \\ & + (2c_3c_1b_3b_1/\langle b\rangle^2)S_{31}(Q) \end{aligned} \tag{2}$$

where

$$\langle b\rangle = \sum_{i=1,2,3}^{m} c_ib_i \qquad \langle b^2\rangle = \sum_{i=1,2,3}^{m} c_ib_i^2$$

are the average coherent scattering length and its mean square value respectively; c_i and b_i are the atomic concentration and the coherent scattering length of the ith element and W_{ij} is the pair contribution of atoms i, j or the weight of the partial factor S_{ij} (see table 1). To extract exactly the complete set of $S_{ij}(Q)$ functions six experiments with different W_{ij} are necessary; in this work we have only the global $S(Q)$.

The total pair correlation function is obtained by a Fourier transformation of the reduced function to real space:

$$G(r) = \frac{2}{\pi}\int_{Q_{min}}^{Q_{max}} Q(S(Q) - 1)\sin(Qr)\,dQ \tag{3}$$

which gives the radial distribution function (RDF) as

$$\mathrm{RDF}(r) = 4\pi r^2\rho_0 + rG(r) = 4\pi r^2\rho(r) \tag{4}$$

where ρ_0 is the mean number density expressed in atoms $Å^{-3}$ and $\rho(r)$ the atomic distribution function.

The exact coordination numbers are obtained by integration of the peaks of the partial radial distribution functions $\mathrm{RDF}_{ij}(r)$. For instance the atoms contained in the nth shell are given as follows:

$$Z_{ij}^n = c_j\int_{r_{ij_{min}}^n}^{r_{ij_{max}}^n} \mathrm{RDF}_{ij}(r)\,dr \tag{5}$$

where $r_{ij_{min}}^n$ and $r_{ij_{max}}^n$ are the lower and upper limits of the nth shell defined by the minima of RDF_{ij}; Z_{ij} is the average number of atoms j in the shell around an atom of type i at the origin and the average distance between atoms i and j is given by $r_{ij} = (r_{ij_{(max)}} + r_{ij_{(min)}})^{1/2}$ if the distribution can be approximated by a discrete Gaussian [19]. Here only the peaks of the total function (RDF) will be considered and partial coordination numbers estimated from simplifying assumptions.

4. Results

4.1. General observations

The sample scattering $I_S(2\Theta)$ is calculated using the procedure previously described [15] and applied to the raw intensities $I_{SCFB}(2\Theta)$, $I_{CFB}(2\Theta)$ and $I_{FB}(2\Theta)$ where the symbols S, C, F and B represent the sample, container, furnace and background respectively. Correction of the container Bragg peaks is not accurately achieved by this method. Moreover, due to the recrystallization of the Pt, which is not fully controlled, it is also necessary to correct for any excess diffuse scattering at the foot of the peaks. In the case of a well isolated peak, errors in the correction appear as a sharp feature in the curve which is easily erased. If several reflections, close to each other, are present, their correction is more complicated. In practice, we assume that the peak shape changes homothetically during recrystallization and that this change is related to the intensity of the variation of the peak maxima. In this manner the parasitic intensity due to recrystallization is accurately recomputed and subtracted (see figure 2).

In the view of their weak variation with temperature, the total $S(Q)$ functions, deduced from equation (1), are shown in figure 3 for only three temperatures. No particular changes are detected at high temperature. In the undercooled domain below 1520 K, weak evolutions are observed as marked by arrows on the pattern at 1490 K which is the most structured. The first peak becomes narrower. The bumps on the broad second peak are enhanced. The third peak develops a shoulder at ~ 8.3 Å^{-1} on the right side of its maximum located at 7.1 Å^{-1}; the slope of its left side is changed and confirms a sharper distribution around 7.1 Å^{-1}. To confirm the variation versus T, the difference $\Delta S(Q) = S(Q)_{T_1} - S(Q)_{T_2}$ was computed for several temperatures T_1 and T_2, with $T_1 > T_2$. At high temperature the $\Delta S(Q)$ values are nearly within statistical errors. The weak features found at 1490 K could not be identified with crystalline niobate.

Figure 4 shows the reduced atomic distribution function $G(r)$ defined by equation (3). The positions of the first, second and third peaks can be considered as independent of temperature; the corresponding interatomic distances are equal to 1.93 ± 0.02 Å, 2.87 ± 0.03 Å and 3.87 ± 0.04 Å respectively. At larger r values, the pattern is more complicated but again rather temperature independent, except for weak features appearing in the supercooled domain as marked by arrows on the 1490 K plot. For $r \geqslant 10$ Å the oscillations are damped to the level of parasitic noise due to cut-off problems of the Fourier transform.

4.2. Determination of the r_{ij} distances and the n_{ij} coordination numbers

The radial distribution functions RDF(r) were calculated from equation (4) using the measured density values [4]. To determine the mean r_{ij} values in the liquid, the type of ij pair concerned and the coordination numbers n_{ij}, we have compared the RDFs with the distances in the crystal, calculated from the atomic coordinates published for the ferroelectric phase at 300 K and corrected for thermal expansion [8, 9]. An example is given in figure 5 using the results at 1573 K; the crystalline distances are marked at the top of the figure with arrows denoting their mean values discernible within the resolution limit ($\Delta r \simeq 0.3$ Å for $Q_{max} = 16$ Å^{-1}).

The first peak, located in the r range corresponding to the Nb–O and Li–O pairs, is fitted with two Gaussians whose mean scattering vectors and mean square deviations $\sigma = \Delta r_{ij}^2$ are given in table 2 for 1573 K. The magnitude of the broadening of the i–j pair distribution $(\Delta r_{ij}^2)^{1/2}$, is thus directly accessible. If the local order of the liquid is similar to that of the

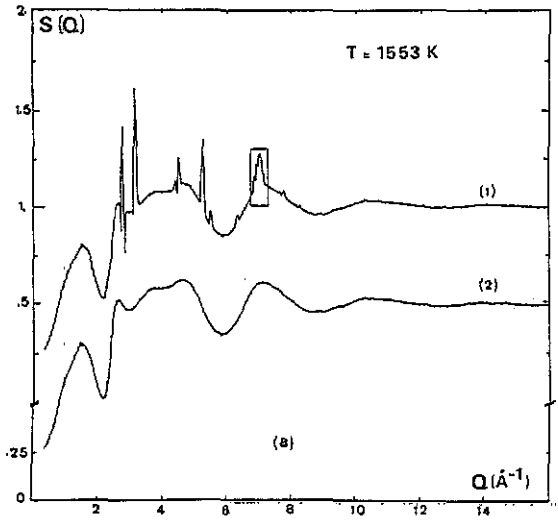

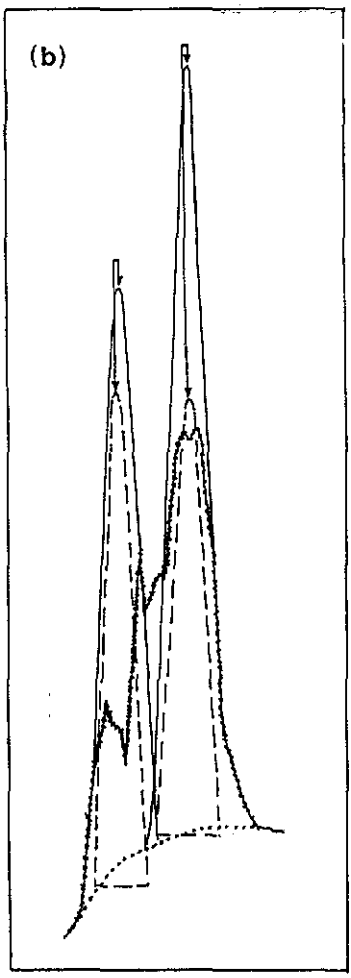

Figure 2. (*a*) Structure factor: curve 1, $S(Q)$ as obtained from the usual correction method [15]; curve 2, $S(Q)$ obtained after a second correction taking recrystallization of Pt into account, see enlargement in (*b*). (*b*) Correction of Pt recrystallization. The triangles show the homothetic rescaling of the peak intensities due to recrystallization. The (331) peak is increased by 1.25, the (420) peak by 1.70. Slight peak position shifts are observed and corrected for. The dotted curve shows the corrected data.

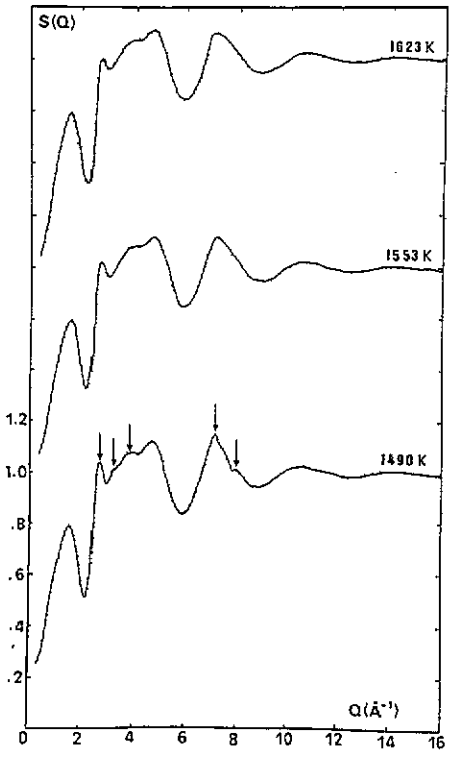

Figure 3. Total structure factors $S(Q)$ at different temperatures; the arrows show the most important changes observed in the pattern at 1490 K.

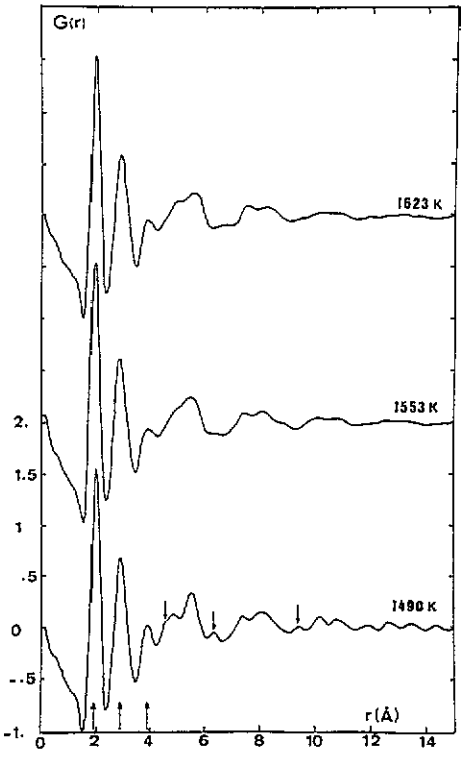

Figure 4. Reduced atomic distribution functions $G(r)$. The up arrows indicate the first three distances.

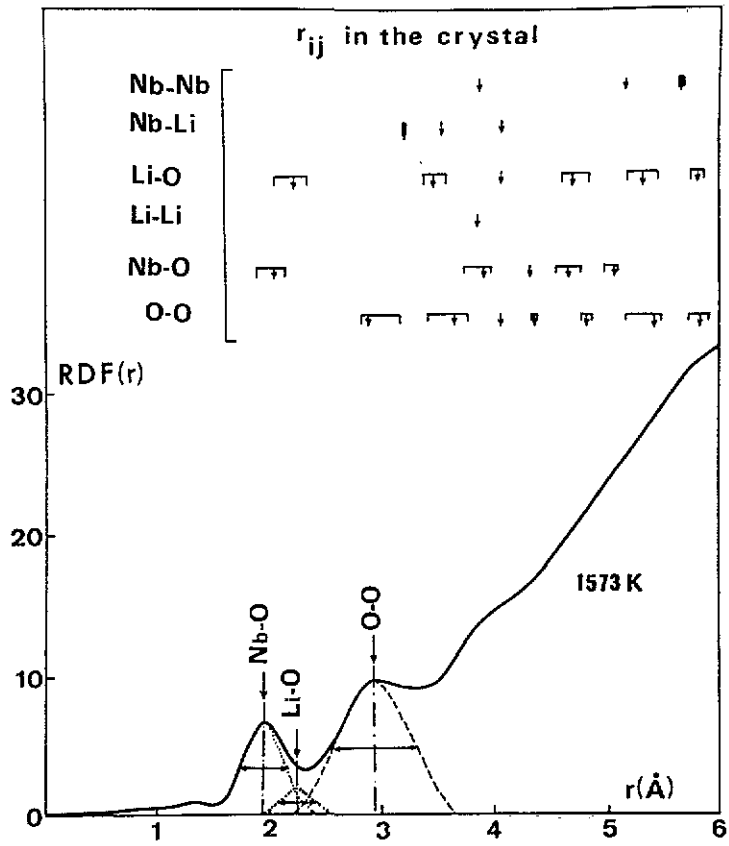

Figure 5. Radial distribution function RDF(r) obtained at 1573 K. The first peak is fitted with two Gaussians corresponding to Nb–O and Li–O contributions and the second peak with a Gaussian corresponding to the O–O contribution.

crystal, the value of Δr_{ij} should be about twice the total spread, Δr_m, observed between the corresponding crystalline r_{ij} distances. The first well defined component is centred on $r_{1_{Nb-O}} \simeq 1.94$ Å and $\Delta r_{ij} = 0.40$ Å, the experimental value being in good agreement with $2\Delta r_m \simeq 2 \times 0.22$ Å. The second component is located at $r_{1_{Li-O}} \simeq 2.16$ Å and its Δr_{ij} value, equal to ~ 0.38 Å, is also in good agreement with $2\Delta r_m = 0.34$ Å.

Table 2. Mean interatomic distances r_{ij} (Å) and mean square deviations σ (Å) used in a fit of the RDF(r) curve at 1573 K and the deduced coordination numbers n_{ij}.

Pairs i–j	r_{ij} (Å)	σ (Å)	n_{ij}
Nb–O	1.94 ± 0.02	0.16	$n_{Nb-O} = 5.9_8 \pm 0.20$
			$n_{O-Nb} = 1.9_9 \pm 0.06$
Li–O	2.16 ± 0.02	0.14	$n_{Li-O} = 2.7_6 \pm 0.10$
			$n_{O-Li} = 0.9_2 \pm 0.04$
O–O	2.88 ± 0.03	0.62	$n_{O-O} = 7.6_0 \pm 0.25$

The second peak is not so well separated; it is fitted by only one component due to the O–O contribution centred at the maximum $r_{1_{O-O}} \simeq 2.88$ Å. Assuming that the local

Table 3. Evolution of $r_{1_{Nb-O}}$ and n_{Nb-O} with temperature.

Temperature (K)	$r_{1_{Nb-O}}$ (Å)	n_{Nb-O}
1490	$1.93_3 \pm 0.02$	$6.0_1 \pm 0.20$
1548	1.93_5 "	6.0_3 "
1553	1.93_3 "	5.9_7 "
1573	1.93_8 "	5.98 "
1623	1.93_7 "	5.94 "
300 (solid)	1.88_9–2.11_2	6.00

orders are similar in the liquid and the crystal, no other contribution should be present at this distance. The Δr_{O-O} value can be evaluated from the HWHM measured on the lower-r side of the peak after subtraction of the Li–O contribution. So $\Delta r_{O-O} = 0.80$ Å, a value slightly higher than the corresponding $2\Delta r_m \simeq 0.72$ Å.

The coordination numbers are then straightforwardly obtained from the areas of the Gaussian components according to $n_{ij} = (c_j/c_i)n_{ji}$. The same analysis is applied at each temperature. When T decreases from 1623 K to 1490 K, only very weak changes are observed in n_{Nb-O} ($5.9_4 \Rightarrow 6.0_3 \Rightarrow \sim 1.5\%$) and $r_{1_{Nb-O}}$ ($1.93_7 \Rightarrow 1.93_3 \Rightarrow \sim 0.3\%$); these deviations (see table 3) are always within our experimental accuracies estimated to $\Delta n/n \leqslant 3\%$ and $\Delta r/r \leqslant 1\%$. With $n_{Nb-O} \simeq 6.0_0 \pm 0.20$, Nb remains octahedrally coordinated in the melt. The averaged $r_{1_{Nb-O}} = 1.93_5 \pm 0.02$ Å has to be compared with the crystalline distances included between 1.8890 Å and 2.1124 Å with a mean value equal to 2.00 Å at 300 K.

The value $n_{Li-O} \simeq 2.8$ can be explained only if a large fraction of Li atoms are bonded with three O atoms and the value $r_{1_{Li-O}} \simeq 2.16 \pm 0.02$ Å has to be compared with the first crystalline r_{Li-O} distances, between 2.0686 Å and 2.2386 Å with a mean value equal to 2.1536 Å at 300 K.

The value $n_{O-O} \simeq 7.6$ is still nearly equal to its crystalline value and the distance $r_{1_{O-O}} \simeq 2.88 \pm 0.03$ Å has to be compared with the first crystalline r_{O-O} distances included between 2.7190 Å and 2.8795 Å with a mean value equal to 2.8564 Å at 300 K.

A rough assessment of the variation of the local order versus T is obtained by comparison of the deviations $\Delta\mathrm{RDF}(r)_{\Delta T} = \mathrm{RDF}(r)_{T_1} - \mathrm{RDF}(r)_{T_2}$ in two T ranges, (see figure 6) as follows:

$$\Delta T_1 = 70 \text{ K at high temperatures (from 1623 K to 1553 K)}$$

with

$$\Delta\rho_{01} = \rho_{01553\text{ K}} - \rho_{01623\text{ K}} = 0.878 \times 10^{-3} \text{ atoms Å}^{-3}$$

and

$$\Delta T_2 = 53 \text{ K near freezing (from 1548 K to 1490 K)}$$

with

$$\Delta\rho_{02} = \rho_{01490\text{ K}} - \rho_{01548\text{ K}} = 0.728 \times 10^{-3} \text{ atoms Å}^{-3}.$$

In the high-T domain, by lowering the temperature, a weak oscillation is observed at $r_{1_{Nb-O}}$ and a second oscillation indicates the evolution of the O–O pair contribution. The third and fourth oscillations are more difficult to explain, since they involve simultaneously different kinds of pair. In the low-T domain, no change is observed in $r_{1_{Nb-O}}$ but the variation in the Li–O contribution indicates an increased bonding by Li; the sharp contribution of the first O–O neighbours and the important increase of the Nb–Nb, Li–Nb and Li–O contributions confirm this tightening.

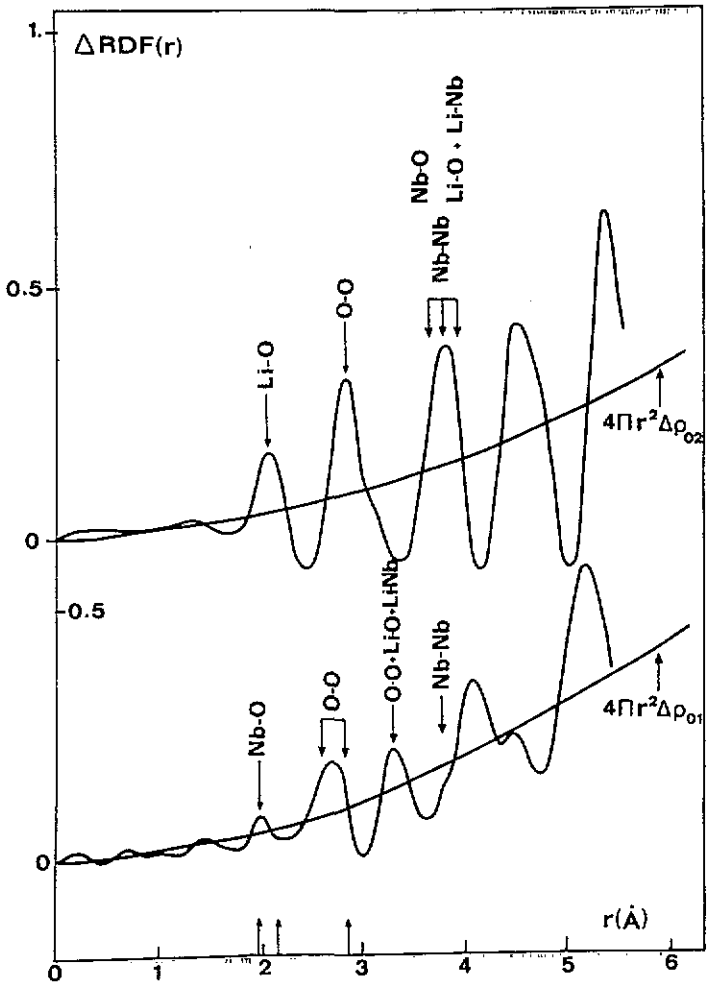

Figure 6. Difference $\Delta_{RDF}(r)$ obtained for two different temperature ranges: $\Delta T_1 = 70$ K from 1623 K to 1553 K (lower curve); $\Delta T_2 = 58$ K from 1548 K to 1490 K (upper curve).

4.3. Discussion

It should be noted that the first interatomic distances in the melt correspond to the mean crystalline values calculated at 300 K without thermal expansion; $r_{1_{Nb-O}}$ is even weakly inferior. The coordination number n_{Nb-O} is also conserved at 6.00 ± 0.20. These results confirm in the melt a local ordering around the Nb atom similar to the crystalline one with a probable presence of octahedral NbO_6 oxide molecules.

In solid networks of linked octahedra, the volume expansion is due to two phenomena: the changes in shape and size of individual octahedra and the changes of their tilt relative to each other. The contribution of the tilt changes to the macroscopic expansion is much greater than that of changes in the octahedron. According to Megaw [9] the mean edge-length thermal coefficient of the octahedron remains small as long as off-centre Nb displacements are present, but it can be large when Nb becomes central as it is in the paraelectric phase. However, the results of this work indicate that the paraelectric behaviour description should be revised, since the mean octahedron size, defined in the rhombohedral state at 300 K,

is maintained in the molten $LiNbO_3$. The rigid octahedral bonds were also confirmed by an EXAFS study of the hydrolysis of niobium pentaethoxide [20] revealing four short Nb–O bonds (1.90 ± 0.03 Å) and two long Nb–O bonds (2.15 ± 0.03 Å); values similar to the crystalline ones. In the melt, more regular NbO_6 octahedra could be present and explain the reduction of the average Nb–O bond.

To explain the increase of Nb–Nb, Li–Nb and Li–O contributions at the lower temperatures, we are led to admit in the melt the existence of aggregates, constituted of corner-sharing NbO_6 octahedra, probably tightened by Li atoms. Our results could be explained by a local atomic arrangement based on the perovskite structure. The presence of clusters in the melt has been recently confirmed by small-angle x-ray scattering [21] and is still being studied.

5. Conclusion

From the *in situ* study of the $LiNbO_3$ melt, the invariability of the n_{Nb-O} coordination has been confirmed in the T range from 1623 K to 1490 K including a large undercooling domain. The coordination numbers n_{Li-O} and n_{O-O} indicate an agglomeration of these octahedra by corner sharing and reinforcement with Li atoms. Cluster models based on NbO_6 arrangements similar to those existing in the crystal should be developed and further investigated.

Acknowledgments

The authors gratefully acknowledge financial support from the Special Coordination Fund for Promotion of Science and Technology granted for the study of the structure of clusters forming melt and its influence on the crystal growth. One of the authors, PA, is indebted for the financial support of an STA fellowship from the Japan International Science and Technology Exchange Centre. Professor Waseda of Tohoku University is thanked for making this collaborative work possible. The samples were prepared at the National Institute for Research in Inorganic Materials in Tsukuba, Japan and the neutron diffraction experiments were carried out at the Institut Laue–Langevin in Grenoble, France.

References

[1] Ballman A A 1965 *J. Am. Ceram. Soc.* **48** 112
[2] Fedolov A, Shapiro Z I and Ladyzhinskii P B 1965 *Sov. Phys.–Crystallogr.* **10** 218 (1965 *Kristallografiya* **10** 268)
[3] Bol'shvov S A, Klyuev V P, Lyapushkin N N, Lyubimov A P and Fedulov S A 1969 *Inorg. Mater. (USSR)* **5** 824–6
[4] Shigematsu K, Anzai Y, Morita S, Yamada M and Yokoyama H 1987 *Japan. J. Appl. Phys.* **26** 1988–96
[5] Ikeda J A S, Fratello V J and Brandle C D 1988 *J. Cryst. Growth* **92** 271–5
[6] Niizeki N, Yamada T and Toyoda H 1967 *Japan. J. Appl. Phys.* **6** 318–27
[7] Voronko Yu K, Kudravtsev A B, Osiko V V and Sobol A A 1988 *Growth of Crystals* vol 16, ed Kh S Bagdasarov and E L Lube (New York: Consultants Bureau) pp 199–217
[8] Abrahams S C, Reddy J M and Bernstein J L 1966 *J. Phys. Chem. Solids* **27** 997–1012
Abrahams S C, Hamilton W C and Reddy J M 1966 *J. Phys. Chem. Solids* **27** 1013–8
Abrahams S C, Levinstein H J and Reddy J M 1966 *J. Phys. Chem. Solids* **27** 1019–26
[9] Megaw H D 1968 *Acta Crystallogr.* A **24** 583–8, 589–604
[10] Aizu K 1965 *Phys. Rev.* **140** 590–6

[11] Smolenskii A, Krainik N N, Kluchua N P, Zhdanova V Y and Mylnikova I E 1966 *Phys. Status Solidi* **13** 309–14
[12] Sugiyama K, Nomura K, Waseda Y, Andonov P, Kimura S and Shigematu K 1990 *Z. Naturf.* a **45** 1325–7
[13] Lerner P, Legras C and Dumas J P 1968 *J. Cryst. Growth* **3/4** 231–5
[14] Bertagnolli H, Chieux P and Zeidler M D 1976 *Mol. Phys.* **32** 759–73
[15] Maret M, Pasturel A, Senillou C, Dubois J M and Chieux P 1989 *J. Physique* **50** 295–310
[16] Koester L and Yelon W B 1983 *Neutron Diffraction Newsletters* The Neutron Diffraction Commission of the International Union of Crystallography
[17] Sears V F 1984 Thermal neutron scattering lengths and cross-sections for condensed material research *AECL Report* 8490
[18] Faber T E and Ziman J M 1965 *Phil. Mag.* **11** 153–73
[19] Busing W R and Levy H A 1962 *Oak Ridge National Laboratory Report* ORNL-TM-271
[20] Vandenborre M T, Poumellec B, Alquier C and Livage J 1989 *J. Non-Cryst. Solids* **108** 333–7
[21] Andonov P, Kimura S, Sawada T and Kobayashi H *Phys. Rev.* submitted